Magneto-optical absorption in an overfilled parabolic quantum well. I. Tilted field

Jed Dempsey and B. I. Halperin
Lyman Laboratory of Physics, Harvard University, Cambridge, Massachusetts 02138
(Received 28 July 1992)

We study the far-infrared optical-absorption spectrum and collective excitations of electrons confined in an imperfect parabolic quantum well in a magnetic field tilted with respect to the growth axis. Using a self-consistent-field approach both with and without a local exchange-correlation potential, we calculate spectra for an "overfilled" well with abrupt boundaries. We choose well parameters to match a real experimental sample, and investigate the effects of well asymmetry and finite temperature on the optical spectrum. We compare our calculations to experiment and find excellent agreement over a wide range of magnetic-field strengths. We also study the effects of overfilling on the low-lying collective excitations, and find that in the sample considered, nonparabolicities are strong enough to shift the energies of the excitations substantially from their ideal-well values.

I. INTRODUCTION

Remotely doped parabolic quantum wells provide an opportunity to study an interacting electron system in the transition region between two and three dimensions.[1–10] By separating the ionized donors by several hundred angstroms from the electrons confined in the well, it is possible to create an almost three-dimensional (3D) electron gas with much weaker electron-impurity interactions than are obtainable in conventional doped semiconductors. In such a system, it might[10] be possible to observe broken-symmetry ground states that have been predicted[11] for the 3D electron gas in the presence of a strong magnetic field. Experimental work has been done on magnetotransport,[1] on magnetocapacitance,[2] on photoluminescence excitation spectroscopy,[3] and on optical and magneto-optical absorption[4–8] in parabolic wells. In the case of perfect parabolic confinement, with an applied magnetic field in a general direction, it has been shown theoretically[12] that long-wavelength optical perturbations can cause transitions only at the two frequencies that correspond to exact excitations in the center-of-mass motion of the electron gas. The substantial agreement between experimental optical spectra[4–6,8] and the distinctive spectrum predicted by theory[12] suggests that the effective confining potential in these samples is indeed nearly parabolic.

In order to observe excitations in the *internal* degrees of freedom of the electron slab, recent optical experiments have studied systems designed to deviate from perfect parabolicity.[6–8] For small deviations, one might expect that nonparabolicity would both shift the excitation energies slightly and redistribute the oscillator strength so that excitations other than the center-of-mass modes become visible in the optical spectrum. For larger deviations, excitations would be shifted substantially from their perfect-well positions, and many peaks of comparable strength would appear in the optical spectrum. Although a detailed study of the dependence of the excitation energies and oscillator strengths on the strength of the nonparabolicity has not yet been made, the general effects of nonparabolicity have been observed in experiments with no magnetic field,[7] and with in-plane[6,8] and tilted[6] magnetic fields, and in calculations of optical spectra for imperfect parabolic wells at $B=0$.[13]

Intersubband optical absorption in quasi-two-dimensional electron systems without[14] and with[15,16] external magnetic fields has been studied by Ando, who used the local-density approximation (LDA) to include exchange and correlation effects within a self-consistent-field (SCF) framework. The picture that emerged from this work[17] is one with absorption peaks near the self-consistent intersubband energy spacings, shifted up slightly by the "depolarization" effect and shifted down slightly by the "excitonlike" correction. In quasi-2D systems, the size of each correction is 10–20 % of the intersubband spacing. Because these corrections are relatively small, and because fully self-consistent calculations are computationally demanding, simple approximation schemes have been used to analyze experimental results in quasi-2D systems,[17] particularly those in tilted magnetic fields.[18]

In remotely doped parabolic wells, however, the picture of shifted intersubband transitions and approximation schemes based on it fail. Because of the parabolic bare potential, Coulomb interactions have a dramatic effect on both the static and the dynamic properties of electrons confined in the well. In the ground state, the electrons form a nearly uniform slab with a width that increases as more electrons are added to the system. The self-consistent potential is nearly flat in the region of the electron slab and, for wide slabs, yields self-consistent energy spacings that are a small fraction of the bare confinement energy $\hbar\omega_0$. In the presence of long-wavelength radiation, the small energy spacings make the electron slab very polarizable, so that intersubband transitions are strongly mixed, forming collective excitations that occur at energies many times larger than the self-consistent energy spacings.[19] The peaks in the absorption spectrum, which correspond to collective excitations, give only obscure information about the intersubband transitions. Indeed, in an ideal parabolic well, absorption

occurs at center-of-mass excitation energies that depend only on $\hbar\omega_0$ and give no information whatsoever about the self-consistent energy spacings. In imperfect parabolic wells, too, depolarization is typically such a strong effect that it is impossible to identify absorption peaks with particular intersubband transitions.

The collective excitations in parabolic wells can be viewed as being midway between intersubband transitions in quasi-2D electron systems and plasmons in three-dimensional systems. In a quasi-2D system, self-consistent screening leads to a small upward shift on the already-large transition energies. In a 3D system, the situation is reversed: there is no gap for particle-hole excitations, and the entire plasmon energy arises from the coherent polarization of the electron gas. In a parabolic well, the electrons are in an intermediate regime where low-energy intersubband transitions are strongly mixed and shifted upward by self-consistent screening. For this reason, a fully self-consistent treatment both of the ground state and of the excitation spectrum is essential.

In a recent paper,[20] the authors reported fully self-consistent calculations of absorption spectra for an imperfect parabolic well in a tilted magnetic field at finite temperature, in which we obtained excellent agreement with experiment over a wide range of magnetic fields. We chose well parameters to match the sample studied experimentally in Ref. 6, and found that finite temperature effects alone could account for the experimental spectrum, without assuming asymmetries in the confining potential. In this paper, we consider the same system—again with a tilted magnetic field—and present detailed calculations of the effects of temperature and of well asymmetries on the optical spectrum. We also calculate and compare the ac density fluctuations associated with the collective modes in the overfilled well to those in an ideal well. In the following paper,[21] we calculate optical spectra for the same overfilled well in the case of in-plane magnetic field. In Sec. II of the present paper, we give details of our method for calculating the self-consistent single-particle eigenfunctions and eigenvalues, the absorption spectrum, and the density fluctuations associated with the collective modes of the system in tilted fields. In Sec. III, we present numerical results for ground-state densities, absorption spectra, and density fluctuations, focusing on the effects of temperature and well asymmetry. In Sec. IV, we summarize the tilted-field results.

II. METHOD

We adapt the method of Ando,[16] and use the SCF approach to calculate the excitation energies, oscillator strengths, and density fluctuations associated with the collective excitations of the system. We first calculate the self-consistent single-particle eigenfunctions and eigenvalues of the system, then use them to find the collective excitations and the self-consistent response of the electron system to incident infrared radiation.

A. Single-particle wave functions and ground-state density

We begin by calculating the self-consistent single-particle wave functions for electrons confined in the z direction by a bare potential that is nearly parabolic, in the presence of a magnetic field tilted at an angle θ with respect to the z axis. We choose the magnetic field to lie in the yz plane, and use the gauge $\mathbf{A}=(zB_y-yB_z,0,0)$. The single-particle Hamiltonian is then

$$\mathcal{H}_0=\frac{(p_x-m^*\omega_{cz}y+m^*\omega_{cy}z)^2}{2m^*}+\frac{p_y^2}{2m^*}+\frac{p_z^2}{2m^*}+V(z)\ , \tag{1}$$

where m^* is the electron effective mass, ω_{cy} and ω_{cz} are eB_y/m^*c and eB_z/m^*c, respectively, and

$$V(z)=V_c(z)+V_H(z)+V_{\rm XC}(z) \tag{2}$$

is the sum of the bare confining potential V_c, the Hartree potential

$$V_H(z)=-\frac{2\pi e^2}{\epsilon_{\rm sc}}\int_{-\infty}^{\infty}dz'\,n(z')|z-z'|\ , \tag{3}$$

and a local exchange-correlation potential[22]

$$V_{\rm XC}(z)=-0.985\frac{e^2}{\epsilon_{\rm sc}}n(z)^{1/3}\left[1+\frac{0.022\,85}{a_B^*n(z)^{1/3}}\ln[1+33.852a_B^*n(z)^{1/3}]\right]\ . \tag{4}$$

In these expressions, $-e$ is the electron charge, $n(z)$ is the electron density, $\epsilon_{\rm sc}$ is the dielectric constant of the host semiconductor, and $a_B^*\equiv\epsilon_{\rm sc}\hbar^2/m^*e^2$ is the effective Bohr radius.

Because $[\mathcal{H}_0,p_x]=0$, we can write the eigenfunctions of $\mathcal{H}_0$ in the form

$$\psi_{\mu Y}(x,y,z)=\frac{e^{iYx/l_1^2}}{\sqrt{L_x}}\phi_\mu(y-Y,z) \tag{5}$$

and apply periodic boundary conditions in the x direction. $\phi_\mu(y,z)$ satisfies the nonseparable partial differential equation

$$\mathcal{H}_{\rm eff}\phi_\mu=\varepsilon_\mu\phi_\mu \tag{6}$$

where ε_μ—independent of Y—is the eigenvalue of $\mathcal{H}_0$ belonging to $\psi_{\mu Y}$. We write the effective Hamiltonian $\mathcal{H}_{\rm eff}$ as the sum of three terms:

$$\mathcal{H}_y=\frac{p_y^2}{2m^*}+\tfrac{1}{2}m^*\omega_{cz}^2y^2\ , \tag{7}$$

$$\mathcal{H}_z=\frac{p_z^2}{2m^*}+\tfrac{1}{2}m^*\omega_{cy}^2z^2+V(z)\ , \tag{8}$$

$$\mathcal{H}_{yz} = -m^* \omega_{cy} \omega_{cz} yz \ , \tag{9}$$

and expand ϕ_μ in a basis formed from direct products of the (real, normalized) eigenfunctions of $\mathcal{H}_y$ and $\mathcal{H}_z$:

$$\phi_\mu(y,z) = \sum_{Nm} S_{Nm,\mu} \chi_N(y) \xi_m(z) \ , \tag{10}$$

where

$$\mathcal{H}_y \chi_N(y) = (N + \tfrac{1}{2}) \hbar \omega_{cz} \chi_N(y) \ , \tag{11}$$

$$\mathcal{H}_z \xi_m(z) = \varepsilon_m \xi_m(z) \ . \tag{12}$$

$\mathcal{H}_y$ is the Hamiltonian for an harmonic oscillator, and we can write χ_N explicitly as

$$\chi_N(y) = \frac{1}{(2^N N! \pi^{1/2} l_\perp)^{1/2}} H_N(y/l_\perp) e^{-(1/2)y^2/l_\perp^2} \ , \tag{13}$$

where H_N is a Hermite polynomial and $l_\perp = (\hbar/m^* \omega_{cz})^{1/2} = (eB_z/\hbar c)^{1/2}$ is the effective magnetic length in the xy plane.

In this basis, the matrix elements of $\mathcal{H}_0$ are

$$\langle NmY|\mathcal{H}_0|N'm'Y'\rangle = \delta_{YY'}\{[(N+\tfrac{1}{2})\hbar\omega_{cz} + \varepsilon_m]\delta_{NN'}\delta_{mm'} + \langle NmY|\mathcal{H}_{yz}|N'm'Y\rangle\} \ , \tag{14}$$

where

$$\langle NmY|\mathcal{H}_{yz}|N'm'Y\rangle = -m^* \omega_{cy} \omega_{cz} z_{mm'} [\sqrt{N+1}\,\delta_{N',N+1} + \sqrt{N}\,\delta_{N',N-1}] \tag{15}$$

and $z_{mm'} = \int dz\, \xi_m(z) z \xi_{m'}(z)$. The coefficients $\{S_{Nm,\mu}\}$ form a real orthogonal matrix that diagonalizes $\mathcal{H}_0$,

$$(S^{-1}\mathcal{H}_0 S)_{\mu\nu} = \varepsilon_\mu \delta_{\mu\nu} \ . \tag{16}$$

If we define

$$\rho_{\mu\nu} \equiv 2\pi l_\perp^2 \sum_Y \psi^*_{\mu Y}(\mathbf{r}) \psi_{\nu Y}(\mathbf{r}) \ , \tag{17}$$

and use the relation

$$\lim_{L_x \to \infty} \frac{1}{L_x} \sum_Y \chi_N(y - Y) \chi_{N'}(y - Y) = \frac{1}{2\pi l_\perp^2} \delta_{NN'} \ , \tag{18}$$

we can write the ground-state density as

$$n_0(z) = \frac{g_s}{2\pi l_\perp^2} \sum_\nu f(\varepsilon_\nu) \rho_{\nu\nu}(z) \ , \tag{19}$$

where

$$\rho_{\mu\nu}(z) = \sum_{Nm} \sum_{N'm'} S_{Nm,\mu} S_{N'm',\nu} \xi_m(z) \xi_{m'}(z) \delta_{NN'} \ , \tag{20}$$

$f(\varepsilon) = (\exp[(\varepsilon - \mu)/k_B T] + 1)^{-1}$ is the Fermi function, and g_s is the spin degeneracy. The chemical potential μ is fixed by the relation $n_s = (g_s/2\pi l_\perp^2) \sum_\nu f(\varepsilon_\nu)$.

B. Absorption and collective modes

Having calculated the self-consistent single-particle eigenfunctions and eigenvalues, we can calculate the absorption spectrum. Because the radiation in the experiment of Ref. 6 is normally incident and unpolarized,[23] we want the xx and yy components of the modified two-dimensional conductivity $\tilde{\sigma}^{2D}$. Ando[16] and Zaluzny[24] have shown that the zz (Ref. 16) and yy (Ref. 24) components of $\tilde{\sigma}^{2D}$ can be written

$$\tilde{\sigma}^{2D}_{ii}(\omega) = -i\omega e^2 \left[\frac{\hbar^2}{2m^*}\right] \sum_\eta \frac{f^{(i)}_\eta}{\tilde{\varepsilon}^2_\eta - (\hbar\omega)^2 - 2i\hbar\omega(\hbar/\tau)} \ , \tag{21}$$

where

$$f^{(i)}_\eta \equiv \left[\sum_{\mu\nu} U_{\mu\nu,\eta} \left[\frac{2m\varepsilon_{\mu\nu}}{\hbar^2}\right]^{1/2} \left[\frac{g_s}{2\pi l_\perp^2}\right]^{1/2} \times [f(\varepsilon_\nu) - f(\varepsilon_\mu)]^{1/2} \langle \mu|x_i|\nu\rangle\right]^2 \tag{22}$$

and $i = \{y,z\}$. In these expressions, $\varepsilon_{\mu\nu} \equiv \varepsilon_\mu - \varepsilon_\nu, \tau$ is a phenomenological relaxation time, and $\{\tilde{\varepsilon}^2_\eta\}$ and $\{U_{\mu\nu,\eta}\}$ are the eigenvalues and eigenvectors of the matrix

$$\Lambda_{\mu\nu,\mu'\nu'} = \varepsilon^2_{\mu'\nu'} \delta_{\mu\mu'} \delta_{\nu\nu'} + \frac{g_s}{2\pi l_\perp^2} \varepsilon^{1/2}_{\mu\nu} [f(\varepsilon_\nu) - f(\varepsilon_\mu)]^{1/2} (\alpha_{\mu\nu,\mu'\nu'} - \beta_{\mu\nu,\mu'\nu'}) [f(\varepsilon_{\nu'}) - f(\varepsilon_{\mu'})]^{1/2} \varepsilon^{1/2}_{\mu'\nu'} \ . \tag{23}$$

Depolarization ($\alpha_{\mu\nu,\mu'\nu'}$) and excitonlike ($\beta_{\mu\nu,\mu'\nu'}$) effects are included through

$$\alpha_{\mu\nu,\mu',\nu'} = -\frac{4\pi e^2}{\epsilon_{sc}} \int_{-\infty}^{\infty} dz\, \rho_{\mu\nu}(z) \int_{-\infty}^{z} dz' \int_{-\infty}^{z'} dz'' \rho_{\mu'\nu'}(z'') \tag{24}$$

and

$$\beta_{\mu\nu,\mu'\nu'} = -\int_{-\infty}^{\infty} dz\, \rho_{\mu\nu}(z) \frac{\delta V_{XC}}{\delta n} \rho_{\mu'\nu'}(z) \ , \tag{25}$$

and the oscillator strengths $\{f^{(i)}_\eta\}$ satisfy the sum rule $\sum_\eta f^{(i)}_\eta = 1$. We point out that we have chosen phase conventions such that $U_{\mu\nu,\eta}$ and the matrix elements $\langle \mu|x_i|\nu\rangle$ for $i = \{y,z\}$ are real.

Because of the tilted magnetic field, light polarized along the x direction will couple to the same collective excitations, with the same energies $\{\tilde{\varepsilon}_\eta\}$, as light with y or z polarization. To calculate $\tilde{\sigma}^{2D}_{xx}$, however, the formulation of Ando[16] in terms of a scalar perturbing potential is inconvenient. Instead, we consider the response to an external vector potential in the x direction, and obtain the general result (valid at finite frequency)

$$\mathrm{Re}\tilde{\sigma}_{xx}^{2\mathrm{D}}=\frac{\omega_c^2}{\omega^2}\mathrm{Re}\tilde{\sigma}_{\hat{n}\hat{n}}^{2\mathrm{D}} , \tag{26}$$

where $\hat{\mathbf{n}}=\hat{\mathbf{B}}\times\hat{\mathbf{x}}=\hat{\mathbf{y}}\cos\theta-\hat{\mathbf{z}}\sin\theta$. Using our knowledge of the excitation energies $\{\tilde{\varepsilon}_\eta\}$, we obtain the oscillator strengths for x polarization,

$$f_\eta^{(x)}\equiv\left[\frac{\hbar\omega_c}{\tilde{\varepsilon}_\eta}\sum_{\mu\nu}U_{\mu\nu,\eta}\left[\frac{2m\varepsilon_{\mu\nu}}{\hbar^2}\right]^{1/2}\left[\frac{g_s}{2\pi l_\perp^2}\right]^{1/2}[f(\varepsilon_\nu)-f(\varepsilon_\mu)]^{1/2}[\cos\theta\langle\mu|y|\nu\rangle-\sin\theta\langle\mu|z|\nu\rangle]\right]^2 . \tag{27}$$

The relation in Eq. (26) is derived in the Appendix.

Also of interest are the ac density fluctuations $n_1(z)$ associated with the collective excitations of the system. For the excitation at $\tilde{\varepsilon}_\eta$, the form factor $n_1(z)$ can be written

$$n_1(z)\propto\sum_{\mu\nu}\varepsilon_{\mu\nu}^{1/2}[f(\varepsilon_\nu)-f(\varepsilon_\mu)]^{1/2}\rho_{\mu\nu}(z)U_{\mu\nu,\eta} . \tag{28}$$

III. RESULTS

As in Ref. 20, we calculate optical spectra for two wells: one well designed to be identical to the nominally 750-Å-wide well in the sample of Ref. 6, and one well with the same curvature but with perfect parabolicity. The two wells are shown schematically in Fig. 1. The experimental sample used in Ref. 6 was cut from a wafer grown to have a well width of 750 Å and an Al concentration that varied quadratically from $x=0$ at the center of the well to $x=0.1$ at the well boundary, where the concentration jumped discontinuously to $x=0.3$. Thick Si-doped layers were set back 200 Å from the well on both sides.[25] Because the Al profile in unrotated molecular-beam-epitaxy samples like that used in Ref. 6 can vary across the wafer,[26] and because the conduction-band offset in $Al_xGa_{1-x}As$ is somewhat uncertain, the potential profile for the experimental sample is not known precisely. To obtain a quantitative match between theory and experiment, we use well parameters that lie within the various uncertainties: width 787.5 Å, parabolic height 70 meV, and additional potential discontinuity 150 meV. The sheet density of carriers was measured[27] to be $n_s=4.7\times10^{11}$ cm^{-2} which, for the present, we shall assume to come equally from the donors on each side of the well and to be independent of magnetic-field strength. We use the tilt angle 23° specified in Ref. 6 and an effective mass $m^*=0.07m_e$, which represents an average over the width of the well.

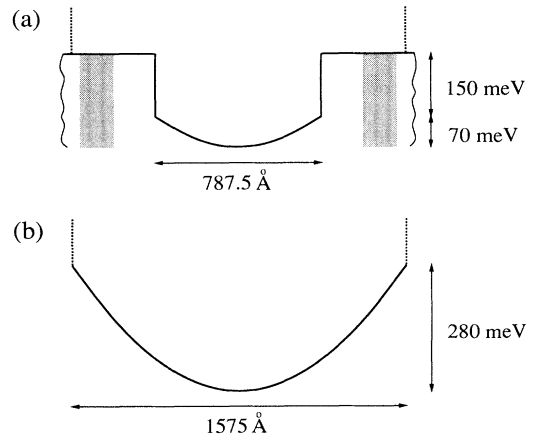

FIG. 1. Schematic representation of the two model wells considered. The well in (a) is designed to be identical to the nominally 750-Å-wide well studied in Ref. 6. We use a well width of 787.5 Å, and a parabolic height of 70 meV. We use donor layers that are 160 Å wide, set back symmetrically 200 Å from the well on both sides. The well in (b) is a model of an idealized well with the same curvature but perfect parabolicity. In practice, the calculations for both wells use infinite walls at $z=\pm787.5$ Å, which are indicated by vertical dotted lines.

The main computational difficulty in doing self-consistent calculations with a tilted magnetic field is the nonseparable partial differential equation, Eq. (6), that must be solved at each iteration in the approach to self-consistency. In our calculations of the self-consistent single-particle eigenfunctions and energies at each value of the magnetic field, we diagonalize the effective Hamiltonian in the basis $\{\chi_N(y),\zeta_m(z)\}$ described in Sec. II A. In the calculations presented here, we have truncated the basis at 200, using the Nm combinations with the lowest combined energies $(N+\frac{1}{2})\hbar\omega_{cz}+\varepsilon_m$. We find that this gives convergence in the eigenvalues $\{\varepsilon_\mu\}$ to one part in 10^5 for the lowest 20 eigenfunctions. The actual confining potentials $V_c(z)$ we use for both model wells have infinite walls at $z=\pm787.5$ Å, which have negligible effects on our results. In calculating the absorption, we consider all transitions between the lowest 20 eigenlevels.

A. Perfect well

As a check of our calculational techniques, we first consider the well with perfect parabolicity. In this case, we know from the generalized Kohn's theorem[12] that absorption should take place only at the two center-of-mass (CM) mode frequencies

$$\omega_\pm^2=\tfrac{1}{2}(\omega_0^2+\omega_c^2)\pm\tfrac{1}{2}[(\omega_0^2+\omega_c^2)^2-4\omega_0^2\omega_{cz}^2]^{1/2} , \tag{29}$$

and that for normally incident unpolarized light the oscillator strengths of the two modes should be

$$f_+=\tfrac{1}{2}(f_+^{(y)}+f_+^{(x)})=\frac{1}{2}\left[\sin^2\alpha+\frac{(\omega_{cy}\cos\alpha+\omega_{cz}\sin\alpha)^2}{\omega_+^2}\right] , \tag{30}$$

$$f_- = \tfrac{1}{2}(f_-^{(y)} + f_-^{(x)})$$
$$= \frac{1}{2}\left[\cos^2\alpha + \frac{(\omega_{cy}\sin\alpha - \omega_{cz}\cos\alpha)^2}{\omega_-^2}\right], \quad (31)$$

where the angle α is defined[12] by $\tan 2\alpha = 2\omega_{cy}\omega_{cz}/(\omega_0^2 + \omega_{cy}^2 - \omega_{cx}^2)$.

Figure 2 shows the ground-state electron density and self-consistent potential for the ideal parabolic well at 12 T in the Hartree approximation (where V_{XC} is omitted). At this large magnetic field, the charge density in the center of the well is quite uniform, and takes a value slightly larger than the design density $\bar{n}_0 = (\epsilon_{xc} m^* \omega_0^2/4\pi e^2)$ because of the magnetic field. Because the parabolic potential is relatively "soft," the density is appreciable out to $z = \pm 500$ Å, even though the nominal slab width is $n_s/\bar{n}_0 = 2 \times 362.25$ Å. The self-consistent potential is smooth, with minima near the edges of the electron slab and a maximum at the center of the well. As the magnetic field is increased, the width of the electron slab shrinks, the density of electrons in the central region increases, and the height of the central maximum of the self-consistent potential increases.

In Fig. 3(a), we show the absorption spectrum calculated for the idealized well using the method of Sec. II, and compare it to the requirements of the generalized Kohn's theorem, Eqs. (29)–(31). The spectrum shown is calculated in the random-phase approximation (RPA), where V_{XC} and $\beta_{\mu\nu,\mu'\nu'}$ are omitted. Our calculated spectrum is shown as filled circles, with the area of each circle proportional to the calculated oscillator strength. The center-of-mass-mode frequencies are shown as solid lines. In Fig. 3(a), we see that the calculated RPA spectrum for the idealized well matches the exact excitation frequencies expected from Kohn's theorem. In fact, the RPA frequencies and oscillator strengths agree to one part in 10^4, except at very high fields, where numerical problems associated with calculating $\zeta_m(z)$ for large m cause small deviations from the Kohn's theorem predictions.

To underline the strength of the depolarization effect in parabolic wells, and the importance of self-consistency in calculating the optical response, we show in Fig. 3(b) the spectrum that results if the self-consistent single-particle eigenfunctions and eigenenergies are used, but the response is calculated without taking into account the self-consistent polarization of the electron slab; that is, without including $\alpha_{\mu\nu,\mu'\nu'}$. Instead of peaks only at the center-of-mass-mode frequencies, as required by Kohn's theorem, one finds many peaks at any given field. Furthermore, the peaks away from the cyclotron frequency appear at frequencies far below the correct center-of-mass-mode frequencies. This is a dramatic illustration of the importance of the depolarization effect in parabolic wells. Not only are some of the excitation energies shifted up by a large factor by the inclusion of depolarization, in fact they coalesce in an ideal parabolic well into a simple two-peak spectrum.

When V_{XC} and $\beta_{\mu\nu,\mu'\nu'}$ are included in our calculations, the results are very similar to those shown in Figs. 2 and 3(a). The inclusion of V_{XC} leads to a ground-state charge

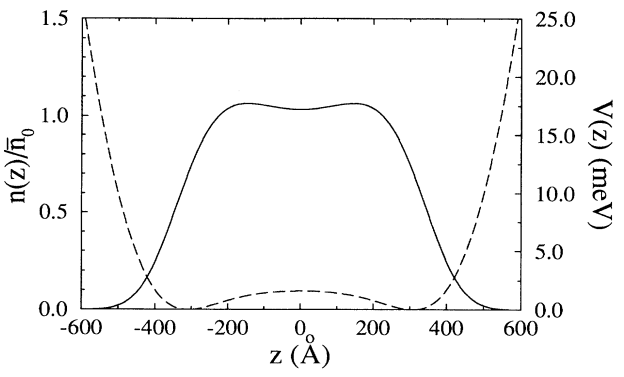

FIG. 2. Ground-state electron density (solid line, left scale) and self-consistent potential (dashed line, right scale) calculated in the Hartree approximation for the ideal parabolic well at $B = 12$ T.

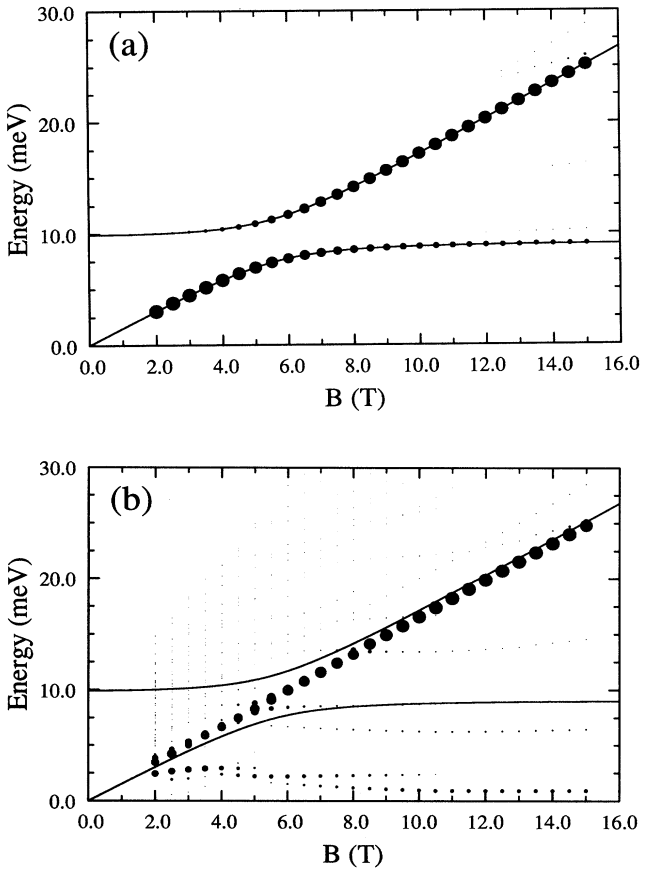

FIG. 3. (a) Comparison of the numerically calculated far-infrared absorption spectrum for an ideal parabolic well in a tilted magnetic field, with the positions predicted by the generalized Kohn's theorem (Ref. 12). The present calculation is shown as filled circles, with the area of each circle proportional to the calculated oscillator strength. (b) Calculated optical spectrum for an ideal parabolic well ignoring the depolarization effect. In this and in all succeeding figures, the tilt angle of the magnetic field is 23° from the sample normal and the spectra shown are for normally incident, unpolarized radiation.

density that is less uniform at 12 T than the Hartree ground state shown in Fig. 2, with larger maxima near $z = \pm 200$ Å. The LDA-SCF absorption spectrum has the same level of agreement with Kohn's theorem as the RPA spectrum shown in Fig. 3(a). In general, we have found that LDA-SCF spectra for imperfect wells, too, are nearly identical to spectra calculated in the RPA, with peak positions differing at most by 3–4%. This is evidence that while depolarization effects are large in parabolic wells, excitonlike effects—at least those calculated using a zero-field local exchange-correlation potential—are small in comparison. This is much different from the situation in quasi-2D systems, where depolarization and excitonlike effects are of comparable magnitude. Because the differences between LDA-SCF and RPA spectra are small, and because the validity of the zero-field exchange-correlation potential V_{XC} is doubtful at high magnetic fields, we show only Hartree-RPA results in our figures unless explicitly indicated.

B. Overfilled well

Now we consider a parabolic well designed to match that used in the experiments of Ref. 6. As mentioned above, we take the width of the well to be 787.5 Å, which is 5% larger than the nominal width of 750 Å, and we take the height of the parabola to be 70 meV, which corresponds to a conduction-band offset of 0.56, assuming that the change in the aluminum concentration from the center to the edge of the well has its design value $\Delta x = 0.1$. Taken together, these assumptions reduce the natural frequency ω_0 of the well by 10% compared to the value it would have with the nominal width and a conduction-band offset of 0.6, and by 17% compared to its value with the nominal width and a conduction-band offset of 0.7. In Fig. 4, we compare the center-of-mass-mode frequencies, shown as solid lines, to the experimental data of Wixforth *et al.*,[6] shown as open boxes. A larger value of ω_0 would lead to CM-mode frequencies that were everywhere higher than those shown. We shall see that overfilling leads to a slight increase in the resonance frequencies near the horizontal portions of the CM-mode frequency curves and to no appreciable change in the portions of the curves that follow the cyclotron resonance. Thus, the experimental data for the CM modes suggest that the actual parameters of the experimental sample have values close to those we use.

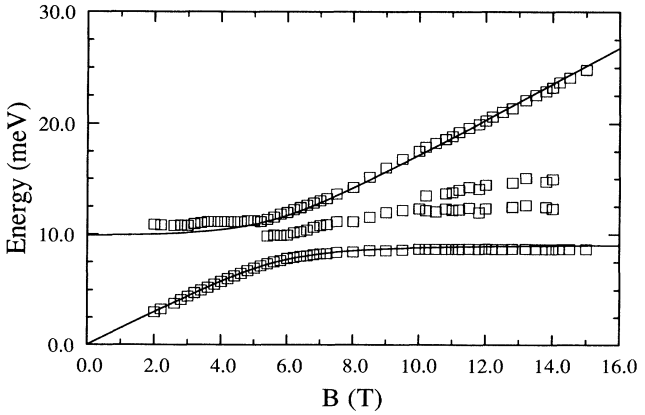

FIG. 4. Comparison of the center-of-mass mode frequencies (solid lines) for our choice of parameters to the experiment of Wixforth *et al.* (Ref. 6) (open boxes). Agreement over a wide range of magnetic fields puts strong constraints on ω_0.

1. Symmetric well, zero temperature

We begin by studying the system at $T = 0$, and by assuming that the confining potential is symmetric about the center of the well. Figure 5 shows the ground-state electron density and the self-consistent potential at 12 T. A comparison with the density for the perfect well shown in Fig. 2 shows that the hard walls at $z = \pm 393.75$ Å have a strong effect on the ground-state density. While the density in the ideal well was appreciable out to $z = \pm 500$ Å, the hard walls in the overfilled well squeeze the electron slab so that its density rises quickly from $z = \pm 400$ Å to a higher average value in the center of the well. Correspondingly, the central maximum in the self-consistent potential has a larger value than in the perfect parabolic well.

In Fig. 6, we compare the calculated absorption spectrum for the imperfect well at $T = 0$ to the CM-mode frequencies. As expected, the imperfect well spectrum has peaks close to the CM-mode frequencies of the perfect well. These peaks are shifted up along the horizontal portions of the CM curves, and follow the CM-mode frequencies closely in the regions near the cyclotron resonance. The upward shift along the horizontal branches is to be expected, since the center-of-mass motion in these regions is predominantly along the z direction, while the motion lies mostly in the xy plane along the cyclotron resonance portions of the curves. One can also view the upward shift as resulting from an increase in the plasma frequency, due to the increase in the average electron density.

In addition to the peaks that lie near the CM-mode frequencies, the nonparabolicities of the confining potential give rise to extra peaks in the absorption spectrum, corresponding to excitations in the internal degrees of freedom

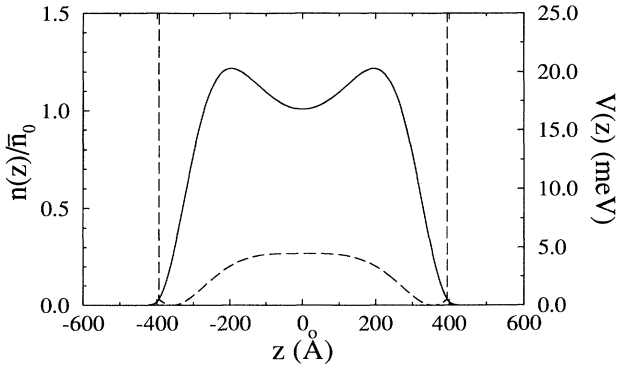

FIG. 5. Ground-state electron density (solid line, left scale) and self-consistent potential (dashed line, right scale) for an imperfect parabolic well at $B = 12$ T. The walls at $z = \pm 393.75$ Å squeeze the ground-state density and lead to a higher average density over the central region of the well.

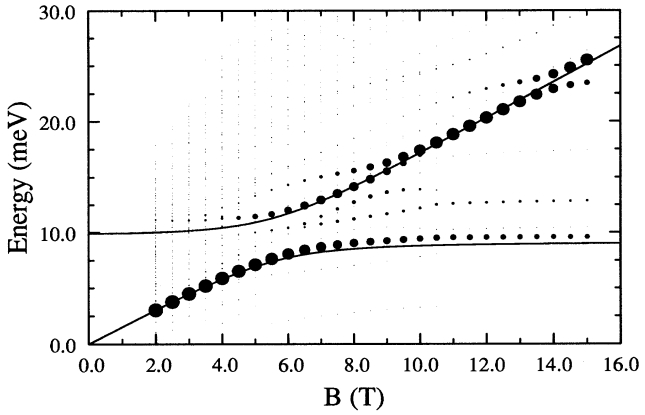

FIG. 6. Comparison of the calculated absorption spectrum for an imperfect well at $T=0$ (filled circles) to the center-of-mass mode frequencies (solid lines). Horizontal portions are shifted up from the CM frequencies because of the increased confinement in the z direction. Extra peaks appear between the two CM modes at large fields, but only one persists to 15 T.

of the electron slab. We call particular attention to the new peaks that lie between the two CM modes in the range from 6 to 15 T. A comparison to the experimental data in Fig. 4 shows that the extra peaks match well with the experimental peaks in the range from 5 to 7 T. Above 10 T, however, the calculated spectrum has only one extra peak, while the experimental data show two. The calculated extra peak lies quite close to the experimental peak near 12.5 meV.

2. *Effects of asymmetry*

One possible origin for the second peak is the presence of asymmetry in the confining potential of the experimental sample. Although the well itself in the experimental sample was grown to be symmetric, differences in the thickness of the donor layers on the two sides of the well and the application of a metallic front gate introduce the possibility that the experimental well has a symmetry-breaking linear term in its confining potential. Even a weak linear potential might produce new peaks in the absorption spectrum, since it would allow transitions that were previously forbidden by symmetry.

To investigate this possibility, we repeat out calculations with a term linear in z added to the bare confining potential. In Fig. 7, we show the self-consistent ground-state density (solid line) and potential (dashed line) in the presence of a linear potential that gives a drop of 20 meV across the width of the well. A potential gradient of this size would result from a difference in donor charge of just a few percent between the layers on either side of the well. One can see that a linear potential of this strength has a substantial effect on the ground-state density, piling up extra charge against the right wall.

In Fig. 8, we compare the absorption spectrum for the asymmetric well to the experimental data. The asymmetry does indeed lead to new peaks that lie between the CM modes at high fields, one near 10 meV and one near 17.5 meV. To make the positions of the new peaks clear,

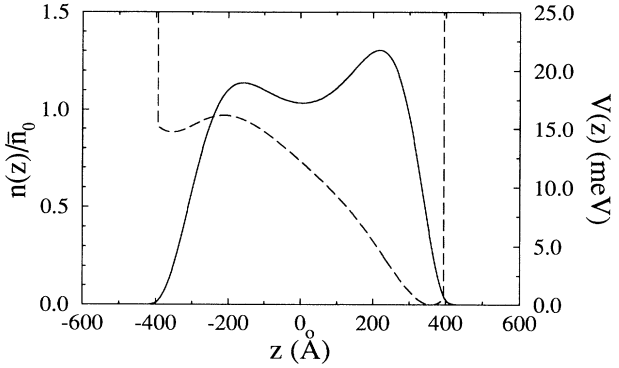

FIG. 7. Ground-state electron density (solid line, left scale) and self-consistent potential (dashed line, right scale) for an imperfect parabolic well in a symmetry-breaking external electric field at $B=12$ T. The electric-field strength corresponds to a voltage drop of 20 mV across the width of the well.

we show them as crosses in Fig. 8. We emphasize that the size of the crosses does not indicate the strength of the new peaks, which have oscillator strengths on the order of 0.001–0.005, an order of magnitude smaller than that of the calculated peak that lies between them. Neither of the two peaks lies near the experimental peak at 15 meV. Furthermore, the two new calculated peaks have nearly equal oscillator strengths, so one would expect either both or neither to be visible in an experiment. We conclude that asymmetry is an unsatisfactory explanation for the second extra peak in the experimental data, since it predicts accurately neither the number of extra peaks nor their positions.

3. *Effects of temperature*

A careful examination of Figs. 6 and 8 suggests another explanation for the second extra peak. In all our calculated spectra, we see two extra peaks in the range from

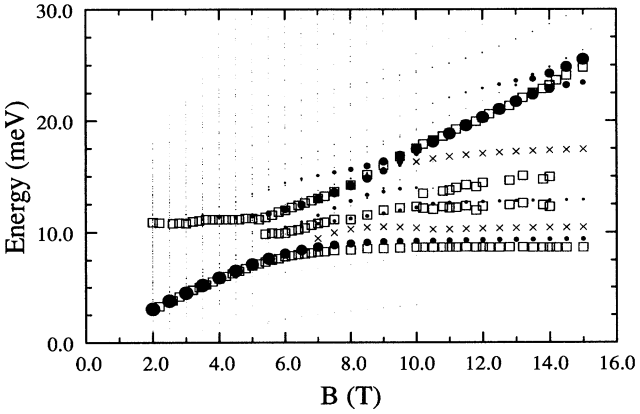

FIG. 8. Comparison of the calculated absorption spectrum for an asymmetric well at $T=0$ (crosses and filled circles) to experimental data of Wixforth *et al.* (Ref. 6) (open boxes). Peaks that are forbidden in a symmetric well (crosses) appear near 10 and 17.5 meV for $B>10$ T, but do not match the peak observed experimentally near 15 meV.

8 to 10 T. Around 10.5 T, however, the oscillator strength in the higher frequency of these two modes goes to zero. The question arises: what happens at 10.5 T?

The answer is that 10.55 T is where the second (ε_1) subband depopulates at zero temperature. The second extra peak in the calculated spectrum arises from transitions from the ε_1 subband to the ε_4 subband, which disappear when the ground-state occupation of the ε_1 subband vanishes. Although the experiments[6] were done at low temperature (4 K), the lowest self-consistent intersubband energy spacing in the well is ~ 1 meV. Because $k_B T$ at 4 K is ~ 0.35 meV, a small ($\sim 10\%$) but significant fraction of the electrons are in the ε_1 subband, even at 15 T.

The presence of these electrons has a strong effect on the absorption spectrum. In Fig. 9, we compare the calculated absorption spectrum for the symmetric overfilled well at $T=4$ K (filled circles) to the experimental data (open boxes). We see that the finite temperature leads to a second extra peak in the calculated spectrum that lies very close to the second extra peak seen in the experiment. In addition, finite temperature introduces *only* this new peak, whereas the symmetry-breaking linear potential considered in the last section leads to two new peaks in the relevant region. We point out that in our calculation the number of electrons in the ε_1 subband drops to zero rapidly as the temperature is reduced from 4 K. Our calculation therefore predicts that the strength of the second extra peak will also vary rapidly in the temperature range from 1 to 4 K.

In Fig. 10, we compare the experimental data (open boxes) to the LDA-SCF absorption spectrum (filled circles) calculated at 4 K. We see that the LDA-SCF spectrum fits experiment well, and does not differ dramatically from the RPA spectrum shown in Fig. 9. The main difference between the LDA-SCF spectrum and the RPA spectrum is that the LDA-SCF calculation places the lower of the two extra peaks 3–4 % lower than the RPA calculation in the range from 8 to 10 T. As discussed in Sec. III A, the similarity between the RPA and the

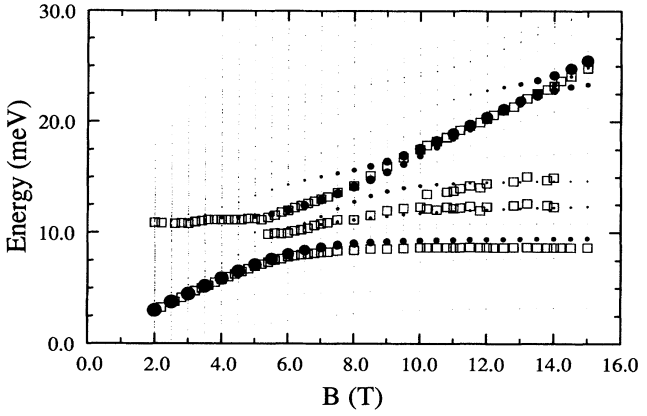

FIG. 9. Calculated RPA absorption for a symmetric well at $T=4$ K (filled circles) vs the experiment of Wixforth *et al.* (Ref. 6) (open boxes). Note the excellent agreement between theoretical and experimental peaks at 12.5 and 15 meV in the region $B > 10$ T.

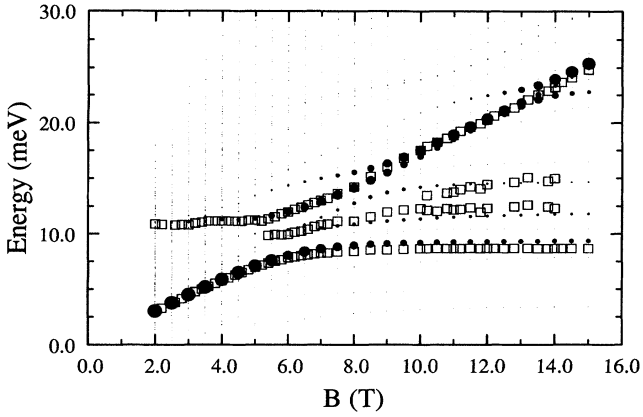

FIG. 10. Calculated LDA-SCF absorption at $T=4$ K (filled circles) vs the experiment of Wixforth *et al.* (Ref. 6) (open boxes). Because the spectrum is dominated by depolarization effects, the LDA-SCF spectrum is very similar to the RPA spectrum shown in Fig. 9.

LDA-SCF spectra suggests that excitonlike effects are small relative to the depolarization effects in parabolic wells.

4. *Strong asymmetry*

As a further and independent check of our understanding of the system, we calculate the spectrum in a case where the well has been partially depopulated by applying a voltage to the front gate. In this situation, the electric field due to the transferred charge adds a strong linear term to the confining potential and makes the well both very asymmetric and, because of the abrupt walls, very nonparabolic. At a gate voltage of -0.7 V, the measured[27] sheet density is 1.87×10^{11} cm^{-2}. From the change in sheet density, we can calculate that the electric field leads to a drop of 205 meV across the well. Because the measured change in sheet density fixes the electric field, there are no new parameters in this new calculation.

The ground-state density (solid line) and self-consistent potential (dashed line) at 12 T are shown in Fig. 11. The

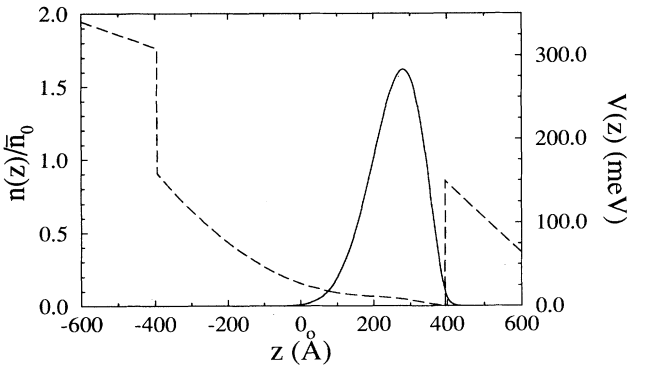

FIG. 11. Ground-state electron density (solid line, left scale) and self-consistent potential (dashed line, right scale) for a partially depopulated well in a strong symmetry-breaking external field at $B=12$ T. The field strength corresponds to a voltage of 205 mV across the width of the well.

confining potential has lost all resemblance to a parabolic potential, and the electron density has a maximum that is more than 1.5 times larger than the design density $\bar{n}_0$ of the well. Calculated and experimental absorption spectra at 4 K are shown in Fig. 12, and we once again see excellent agreement.

C. Collective modes

As a final application, we study the charge-density fluctuations associated with the collective modes of the system. In particular, we focus on the lowest few modes in the high-field regime. In this regime, all the electrons are in the lowest subband at zero temperature, so the spectrum is particularly simple. In Figs. 13 and 14, we show the density fluctuations (solid lines) for the lowest three modes at 12 T for the perfect well at 0 K and the imperfect well at 4 K, respectively. In the perfect well (Fig. 13) only the lowest-energy mode, the center-of-mass mode, is seen in far-infrared absorption. For comparison, we indicate with a dashed line the derivative of the ground-state density shown in Fig. 2. For a rigid translation of the electron slab, the two curves would be identical. The small difference seen here is caused by numerical inaccuracies [associated with calculating $\zeta_m(z)$ for large m] that appear at large fields. The two modes of higher energy can be viewed as slab magnetoplasmons with an increasing quantized wave vector in the z direction. In fact, they are remarkably similar to the plasmon density fluctuations calculated in Ref. 28 using a classical hydrodynamic model and shown in Fig. 13 of Ref. 28.

Figure 14 shows the lowest three collective modes (solid lines) in the imperfect well at 4 K. In the infrared spectrum, the mode in the bottom panel corresponds to the "center-of-mass peak" at 9.5 meV, while the mode in the top panel is the lower of the two extra peaks at 12.5 meV. The mode in the middle panel cannot be excited in a symmetrical well, but becomes visible near 10.8 meV in the presence of a symmetry-breaking electric field. Although the lowest-energy excitation falls near the frequency expected for a perfect well, it is no longer a "center-of-mass" mode, since it does not correspond to a pure translation of the electron slab. This can be seen clearly by comparing the actual density perturbation, shown with a solid line, to the derivative of the ground-state density (see Fig. 5), shown with a dashed line. The

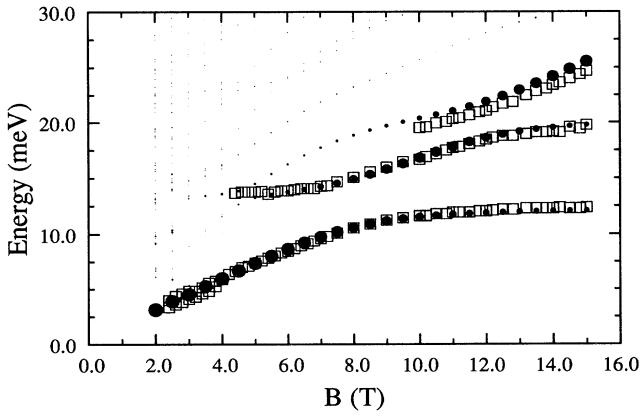

FIG. 12. Comparison of the calculated absorption spectrum for a partially depopulated, strongly asymmetric well (filled circles), with unpublished experimental data provided by Wixforth (open boxes).

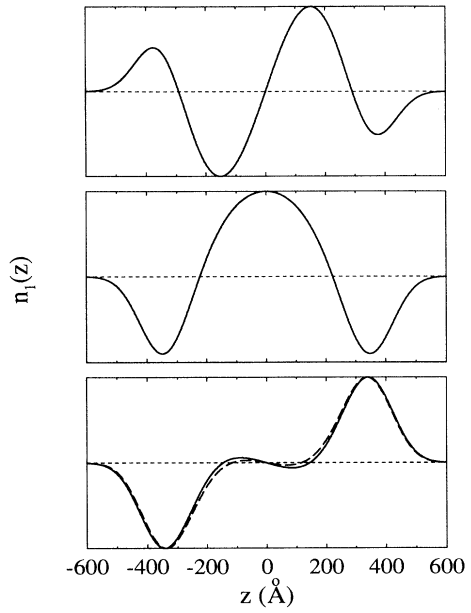

FIG. 13. Density fluctuations $n_1(z)$ for the three lowest collective modes at 12 T in a perfect parabolic well. The dashed line shows the derivative of the ground-state density shown in Fig. 2 for comparison to the center-of-mass mode.

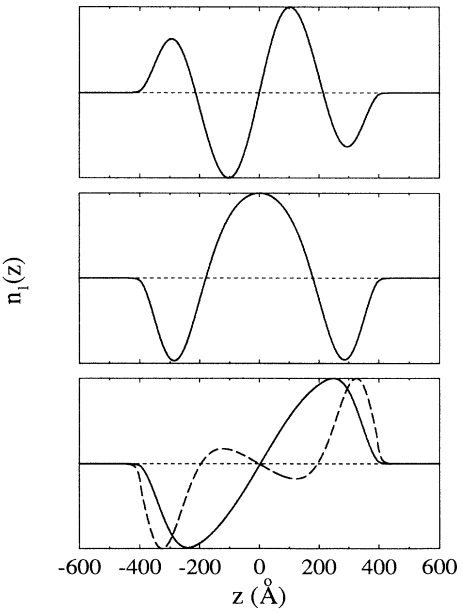

FIG. 14. Density fluctuations $n_1(z)$ for the lowest three collective modes at 12 T in an imperfect parabolic well. The dashed line shows the derivative of the ground-state density shown in Fig. 5 for comparison to the center-of-mass mode.

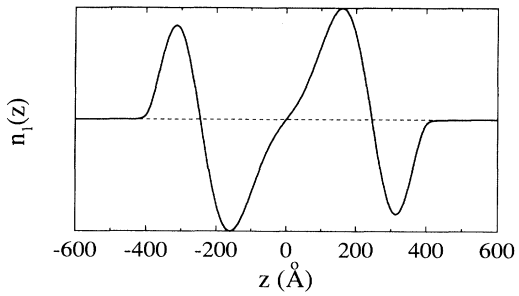

FIG. 15. Density perturbation $n_1(z)$ for the extra excitation that appears at finite temperature. $n_1(z)$ for this mode is very similar to that for the lower-frequency extra excitation, which is shown in the top panel of Fig. 14.

shape of the two higher modes, on the other hand, is not changed dramatically by the hard walls, except that the wavelengths of the fluctuations are reduced. The energies of these excitations, on the other hand, are shifted up substantially from the corresponding values in the perfect well. In the perfect well at 12 T, the three excitations shown have energies 8.94, 9.00, and 9.98 meV. In the imperfect well, the equivalent excitations have energies 9.41, 10.79, and 12.08 meV. Thus we see that the deviations from parabolicity in the imperfect well are sufficient not just to render the internal excitations of the electron slab visible in the optical spectrum, but also to shift their energies substantially.

At finite temperature in the imperfect well, we also excite the mode corresponding to the second extra peak. The density perturbation for this excitation is shown in Fig. 15. Although this mode arises only when the ε_1 subband is occupied, the similarity of its form factor to that of the other "extra peak" (shown in the top panel of Fig. 14) and an examination of the eigenvectors $U_{\mu\nu,\eta}$ shows that it arises from a mixture of $0\rightarrow 3$ and $1\rightarrow 4$ transitions.

IV. SUMMARY

In this paper, we have studied the far-infrared absorption spectrum and the collective excitations of an overfilled parabolic well in a tilted magnetic field using a self-consistent-field approach. We have investigated the effects of well asymmetries and of finite temperatures, and have found that the experimental spectra of Wixforth *et al.*[6] can be understood by including finite temperature effects in calculations on a symmetric well. Our calculations predict that one peak in the spectrum should have a strong temperature dependence in the range from 1 to 4 K. We have also found that the same well parameters that explain the experimental data of Wixforth *et al.* also give excellent agreement with unpublished spectra taken for the same sample in the presence of a strong symmetry-breaking electric field.

Electron-electron interactions are extremely important in parabolic wells, and it is necessary to calculate both the ground state and the response functions self-consistently. We have found that self-consistent screening mixes the intersubband transitions so strongly that it is in general impossible to associate peaks in the absorption spectrum with particular transitions. On the other hand, we have found only small differences between optical spectra calculated in the random-phase approximation and those that include exchange and correlation effects through the local-density approximation. This is in contrast to the situation in quasi-2D electron systems,[17] where the depolarization and excitonlike effects are of comparable magnitude.

We have also studied the effects of overfilling on the low-lying collective excitations of a parabolic well. For the experimental sample we consider, we find that the deviation from parabolicity is sufficiently strong to shift the energies of the excitations substantially, in addition to rendering new excitations visible. It remains to be seen whether the addition of controlled deviations from parabolicity can allow the optical excitation of the internal degrees of freedom of the system without shifting the energies away from their values in the ideal system.

ACKNOWLEDGMENTS

The authors are grateful to B. Y. Gelfand, A. J. Rimberg, P. M. Young, J. H. Burnett, P. F. Hopkins, and M. Sundaram for helpful discussions. We direct special thanks to A. Wixforth for generously providing the data from Ref. 6 shown in Figs. 4, 8, 9, and 10, and the previously unpublished data shown in Fig. 12. Support for this work was provided by the Harvard Materials Research Laboratory under National Science Foundation Grant No. DMR-89-20490.

APPENDIX

We define the modified two-dimensional conductivity $\tilde{\sigma}^{2D}$ and the modified two-dimensional electric susceptibility $\tilde{\chi}^{2D}$ as response functions to a uniform external electric field:

$$\mathbf{J}(\omega)=\tilde{\sigma}^{2D}(\omega)\mathbf{E}^{\text{ext}}(\omega)\ , \tag{A1}$$

$$\mathbf{d}(\omega)=\tilde{\chi}^{2D}(\omega)\mathbf{E}^{\text{ext}}(\omega)\ , \tag{A2}$$

where $\mathbf{J}\equiv\int d^3r\ \mathbf{j}(\mathbf{r})$ is the integrated current density and $\mathbf{d}\equiv\int d^3r\ \mathbf{P}(\mathbf{r})$ is the total electric dipole moment. The relationship $\mathbf{j}=\partial\mathbf{P}/\partial t$ implies that

$$\tilde{\sigma}^{2D}=-i\omega\tilde{\chi}^{2D}\ . \tag{A3}$$

In the presence of a uniform time-dependent external electric field derived from a scalar potential, we can write the perturbing Hamiltonian as

$$\mathcal{H}_1=-\mathbf{d}\cdot\mathbf{E}^{\text{ext}}\ . \tag{A4}$$

If $\mathbf{E}^{\text{ext}}$ is polarized along the $\hat{\mathbf{n}}$ direction, linear-response theory[29] gives the diagonal response at temperature T as

$$\tilde{\chi}^{2D}_{\hat{n}\hat{n}}(\omega)=\frac{1}{\hbar}\sum_{ij}\frac{e^{-\tilde{\varepsilon}_j/k_BT}}{\mathcal{Z}}\left\{\frac{\langle\Psi_j|d_{\hat{n}}|\Psi_i\rangle\langle\Psi_i|d_{\hat{n}}|\Psi_j\rangle}{\omega-\omega_{ij}+i0^+}-\frac{\langle\Psi_j|d_{\hat{n}}|\Psi_i\rangle\langle\Psi_i|d_{\hat{n}}|\Psi_j\rangle}{\omega+\omega_{ij}+i0^+}\right\}, \tag{A5}$$

where $|\Psi_i\rangle$ is an exact many-particle eigenstate of the unperturbed Hamiltonian with energy ε_i, $\tilde{\varepsilon}_i=\varepsilon_i-\mu N_i$, $\omega_{ij}=(\tilde{\varepsilon}_i-\tilde{\varepsilon}_j)/\hbar$, and $\mathcal{Z}=\sum_j e^{-\tilde{\varepsilon}_j/k_BT}$ is the grand-canonical partition function. The electric dipole moment operator is

$$d_{\hat{n}}(\mathbf{r})=(-e)\sum_k \mathbf{r}_k\cdot\hat{\mathbf{n}}\ , \tag{A6}$$

and $\tilde{\chi}^{2D}_{\hat{n}\hat{n}}\equiv\hat{\mathbf{n}}\cdot\tilde{\chi}^{2D}\cdot\hat{\mathbf{n}}$.

When the electric field is polarized along $\hat{\mathbf{x}}$, it is convenient to derive the electric field from an external time-dependent vector potential $A_x^{\rm ext}$ and to define a new response function $\tilde{K}^{2D}$ relating the current to the external vector potential:

$$J_x(\omega)=\tilde{K}^{2D}_{xx}(\omega)\frac{A_x^{\rm ext}(\omega)}{c}\ . \tag{A7}$$

Choosing a gauge with $\phi^{\rm ext}=0$ and using the relation $E_x^{\rm ext}=-(1/c)(\partial A_x^{\rm ext}/\partial t)=i(\omega/c)A_x^{\rm ext}$, we see that

$$\tilde{\sigma}^{2D}_{xx}=\frac{\tilde{K}^{2D}_{xx}}{i\omega}\ . \tag{A8}$$

In this case the perturbing Hamiltonian can be written

$$\mathcal{H}_1=-J_x^{(p)}\frac{A_x^{\rm ext}}{c}+O[(A_x^{\rm ext})^2]\ , \tag{A9}$$

where the operator $\mathbf{J}^{(p)}=(-e/m^*)\sum_k[\mathbf{p}_k+(e/c)\times\mathbf{A}_0(\mathbf{r}_k)]$ plays the role of the paramagnetic current in a system with a uniform B field $\mathbf{B}=\nabla\times\mathbf{A}_0$. Applying linear-response theory once again, we find that $\tilde{K}^{2D}_{xx}$ has two pieces,

$$\tilde{K}^{2D(d)}_{xx}(\omega)=-\frac{e^2}{m^*}N\ , \tag{A10}$$

due to the diamagnetic current (N is the total number of electrons), and

$$\tilde{K}^{2D(p)}_{xx}(\omega)=\frac{1}{\hbar}\sum_{ij}\frac{e^{-\tilde{\varepsilon}_j/k_BT}}{\mathcal{Z}}\left\{\frac{\langle\Psi_j|J_x^p|\Psi_i\rangle\langle\Psi_i|J_x^p|\Psi_j\rangle}{\omega-\omega_{ij}+i0^+}-\frac{\langle\Psi_j|J_x^p|\Psi_i\rangle\langle\Psi_i|J_x^p|\Psi_j\rangle}{\omega+\omega_{ij}+i0^+}\right\}. \tag{A11}$$

Choosing $\mathbf{A}_0=(zB_y-yB_z,0,0)$, and noting that the total canonical momentum in the x direction commutes with the Hamiltonian, we see that

$$\tilde{K}^{2D(p)}_{xx}(\omega)=\omega_c^2\tilde{\chi}_{\hat{n}\hat{n}}(\omega)\ , \tag{A12}$$

provided that $\hat{\mathbf{n}}=\hat{\mathbf{B}}\times\hat{\mathbf{x}}=\hat{\mathbf{y}}\cos\theta-\hat{\mathbf{z}}\sin\theta$. Use of Eqs. (A3) and (A8) allows us to write

$$\tilde{\sigma}^{2D}_{xx}(\omega)=-\frac{e^2}{i\omega m^*}N+\frac{\omega_c^2}{\omega^2}\tilde{\sigma}^{2D}_{\hat{n}\hat{n}}(\omega)\ . \tag{A13}$$

Taking real parts, we obtain Eq. (26).

[1]E.G. Gwinn, R. M. Westervelt, P. F. Hopkins, A. J. Rimberg, M. Sundaram, and A. C. Gossard, Phys. Rev. B **39**, 6260 (1989); M. Shayegan, T. Sajoto, M. Santos, and C. Silvestre, Appl. Phys. Lett. **53**, 791 (1988); T. Sajoto, J. Jo, L. Engel, M. Santos, and M. Shayegan, Phys. Rev. B **39**, 10464 (1989); M. Shayegan, T. Sajoto, J. Jo, and M. Santos, *ibid.* **40**, 3476 (1989); T. Sajoto, J. Jo, M. Santos, and M. Shayegan, Appl. Phys. Lett. **55**, 1430 (1989); E. G. Gwinn, R. M. Westervelt, P. F. Hopkins, A. J. Rimberg, M. Sundaram, and A. C. Gossard, Phys. Rev. B **41**, 10700 (1990); K. Ensslin, M. Sundaram, A. Wixforth, J. H. English, and A. C. Gossard, *ibid.* **43**, 9988 (1991).

[2]A. J. Rimberg, Scott Yang, Jed Dempsey, J. H. Baskey, R. M. Westervelt, M. Sundaram, and A. C. Gossard, Appl. Phys. Lett. **62**, 390 (1993).

[3]J. H. Burnett, H. M. Cheong, W. Paul, P. F. Hopkins, E. G. Gwinn, A. J. Rimberg, R. M. Westervelt, M. Sundaram, and A. C. Gossard, Phys. Rev. B **43**, 12033 (1991).

[4]K. Karrai, H. D. Drew, M. W. Lee, and M. Shayegan, Phys. Rev. B **39**, 1426 (1989).

[5]K. Karrai, X. Ying, H. D. Drew, and M. Shayegan, Phys. Rev. B **40**, 12020 (1989).

[6]Achim Wixforth, M. Sundaram, J. H. English, and A. C. Gossard, in *Proceedings of the 20th International Conference on the Physics of Semiconductors,* edited by E. M. Anastassakis and J. D. Joannopoulos (World Scientific, Singapore, 1990), p. 1705.

[7]A. Wixforth, M. Sundaram, K. Ensslin, J. H. English, and A. C. Gossard, Phys. Rev. B **43**, 10000 (1991).

[8]K. Karrai, X. Ying, H. D. Drew, M. Santos, M. Shayegan, S.-R. E. Yang, and A. H. MacDonald, Phys. Rev. Lett. **67**, 3428 (1991).

[9]B. I. Halperin, Jpn. J. Appl. Phys. **26**, Suppl. 26-3, 1913 (1987).

[10]L. Brey and B. I. Halperin, Phys. Rev. B **40**, 11634 (1989).

[11]V. Celli and N. D. Mermin, Phys. Rev. **140**, A839 (1965); Z. Tesanovic and B. I. Halperin, Phys. Rev. B **36**, 4888 (1987); A. H. MacDonald and G. W. Bryant, Phys. Rev. Lett. **58**, 515 (1987).

[12]L. Brey, N. F. Johnson, and B. I. Halperin, Phys. Rev. B **40**, 10 647 (1989).
[13]L. Brey, Jed Dempsey, N. F. Johnson, and B. I. Halperin, Phys. Rev. B **42**, 1240 (1990); M. P. Stopa and S. Das Sarma, *ibid.* **45**, 8526 (1992). See also, L. Brey, N. F. Johnson, and Jed Dempsey, *ibid.* **42**, 2886 (1990).
[14]T. Ando, Z. Phys. B **24**, 33 (1976).
[15]T. Ando, J. Phys. Soc. Jpn. **44**, 475 (1978).
[16]T. Ando, Phys. Rev. B **19**, 2106 (1979).
[17]T. Ando, A. B. Fowler, and F. Stern, Rev. Mod. Phys. **54**, 437 (1982).
[18]See, for example, G. L. J. A. Rikken, H. Sigg, C. J. G. M. Langerak, H. W. Myron, J. A. A. J. Perenboom, and G. Weimann, Phys. Rev. B **34**, 5590 (1986); A. D. Wieck, F. Thiele, U. Merkt, K. Ploog, G. Weimann, and W. Schlapp, *ibid.* **39**, 3785 (1989); J. J. Koning, R. J. Haug, H. Sigg, K. von Klitzing, and G. Weimann, *ibid.* **42**, 2951 (1990); E. Batke, G. Weimann, and W. Schlapp, *ibid.* **43**, 6812 (1991).
[19]D. A. Broido, P. Bakshi, and K. Kempa, Solid State Commun. **76**, 613 (1990).
[20]Jed Dempsey and B. I. Halperin, Phys. Rev. B **45**, 3902 (1992).
[21]Jed Dempsey and B. I. Halperin, following paper, Phys. Rev. B **47**, 4674 (1993).
[22]We use the local exchange-correlation potential suggested in L. Hedin and B. I. Lundqvist, J. Phys. C **4**, 2064 (1971).
[23]A. Wixforth (private communication).
[24]M. Zaluźny, Phys. Rev. B **40**, 8495 (1989).
[25]M. Sundaram (private communication).
[26]The variation in the Al profile does not degrade the parabolicity of samples cut from the wafer, but causes different samples to have different curvatures. See M. Sundaram, A. Wixforth, R. S. Geels, A. C. Gossard, and J. H. English, J. Vac. Sci. Technol. B **9**, 1524 (1991).
[27]Measured sheet densities provided by A. Wixforth (private communication). The effects of asymmetrical donor charge are discussed in Sec. III B 2.
[28]Jed Dempsey and B. I. Halperin, Phys. Rev. B **45**, 1719 (1992).
[29]See, e.g., *Quantum Theory of Many-Particle Systems* (McGraw-Hill, New York, 1971), Sec. 32.